Journal of
Materials Chemistry C

PAPER

View Article Online
View Journal | View Issue

Cite this: J. Mater. Chem. C, 2015, 3, 4723

A graphene/GaAs near-infrared photodetector enabled by interfacial passivation with fast response and high sensitivity

Lin-Bao Luo,*[a] Han Hu,[a] Xian-He Wang,[a] Rui Lu,[a] Yi-Feng Zou,[a] Yong-Qiang Yu*[a] and Feng-Xia Liang*[b]

Received 14th February 2015,
Accepted 30th March 2015

DOI: 10.1039/c5tc00449g

www.rsc.org/MaterialsC

We report a simple AlO_x passivation approach to optimize the device performance of a bilayer graphene/gallium arsenide (BLG/GaAs) Schottky junction based near infrared photodetector (NIRPD). The as-fabricated NIRPD is highly sensitive to NIR illumination at zero bias voltage, with a detectivity of 2.88×10^{11}, which is much higher than that without passivation (7.3×10^{9} cm $Hz^{1/2}$ W^{-1}). The corresponding responsivity is 5 mA W^{-1}. Additionally, the surface passivation can substantially increase both the response rate (rise/fall time τ_r/τ_f from 32/48 μs to 320/380 ns), and lift time. It is expected that such a self-driven NIRPD with fast response and high detectivity will have great potential in the future optoelectronic devices.

Infrared photodetectors (IRPDs), a kind of commercialized device of great practical importance, have been widely used in various fields, such as missile guidance, astronomy, telecommunications, control systems, and medical diagnostics.[1,2] So far, a variety of IRPDs with different device configurations (*e.g.*, Schottky-barrier photoemissive IRPDs,[3] quantum well IRPDs,[4,5] quantum dot IRPDs[6]) have been developed by using semiconductors with narrow band gap such as ternary semiconductors (*e.g.*, HgCdTe and CdZeTe),[7,8] group III–V (*e.g.* InSb and GaAs) semiconductors,[9–11] and group IV semiconductors (*e.g.* Si and Ge).[12–15] Compared with these traditional devices, photodiode IRPDs have lately received increasing interest due to their simple structures and great performance. For instance, photodiode-based IRPDs have high sensitivity and fast response rate. In addition, these devices normally exhibit typical photovoltaic characteristics, which make it possible to detect light illumination at zero bias voltage.

Gallium arsenide (GaAs), a III–V group compound semiconductor, has a direct bandgap of $\sim$1.42 eV. The narrow bandgap, along with its optimal optoelectronic characteristics and high carrier mobility, has made GaAs an appropriate material for constructing sensitive IRPDs. Wang *et al.* demonstrated an IRPD based on a metal–semiconductor (single GaAs nanowire)–metal Schottky diode structure. The photoconductive gain of the devices approaches 20 000 under low laser excitation.[16] We also reported an n-type GaAs nanocone array/monolayer graphene Schottky junction photodetector. It was observed that the device exhibited high sensitivity to NIR light illumination with a detectivity of 1.83×10^{11} cm $Hz^{1/2}$ W^{-1}.[17] Despite these efforts, it is undeniable that due to lack of effective passivation, these devices normally contain high density of surface states which as carrier trapping centers can pin the surface Fermi level, increase surface recombination and decrease carrier mobility at the GaAs surface.[18] As a result, the GaAs-based devices normally suffer from a low on/off ratio and a slow response rate that constitute the main obstacles to their applications. To solve this issue, people have tried to introduce a passivation layer into the device structure. For example, Liu *et al.* demonstrated a hydrogen peroxide oxidation technique to passivate Al and Ga dangling bonds in an AlGaN/GaN ultraviolet photodetector. Both responsivity and on/off ratio were found to increase dramatically.[19] What is more, Chen *et al.* reported that a thermally evaporated copper phthalocyanine film is effective for passivating surface trap states of ZnO NWs. As a result, the as-passivated photodetector devices exhibit simultaneously improved sensitivity and response rate.[20]

Enlightened by the above studies, we herein present a simple passivation strategy to optimize the bilayer graphene/GaAs wafer (BLG/GaAs) Schottky junction near IRPD (NIRPD). Electrical analysis reveals that the BLG/GaAs Schottky junction with an AlO_x nanofilm retains the typical photovoltaic characteristics after surface passivation. Further optoelectronic characterization demonstrates that both responsivity and detectivity

[a] *School of Electronic Science and Applied Physics Hefei University of Technology, Hefei, Anhui 230009, P. R. China. E-mail: luolb@hfut.edu.cn, yongqiangyu@hfut.edu.cn*
[b] *School of Materials Science and Technology and Anhui Provincial Key Laboratory of Advanced Functional Materials and Devices, Hefei University of Technology, Hefei, Anhui 230009, P. R. China. E-mail: fxliang@hfut.edu.cn*

of BLG/GaAs Schottky NIRPD with AlO_x are much better than those without a passivation layer. The photoresponse rate of the optimized device was also considerably improved from the microsecond to the nanosecond level. This study suggests that the present NIRPD may have great potential in future optoelectronic devices.

BLG films were grown through a chemical vapor deposition (CVD) method using 30 μm thick Cu foils as the catalytic substrates. Briefly, a mixed gas of CH_4 (20 standard cubic centimeters per minute, sccm) and H_2 (40 sccm) as a reaction source was fed into a quartz tube and the base pressure was kept at ~2 Torr. The quartz tube was then heated up to 1005 °C and maintained at this temperature for 20 min. After growth, the graphene films on Cu foils were spin-coated with polymethylmethacrylate (PMMA) solution (6 wt% in anisole). The Cu substrates were then etched away in Marble's reagent solution ($CuSO_4 : HCl : H_2O$ = 10 g : 50 ml : 50 ml). Before transfer of graphene, n-type GaAs wafers ((100) orientation, resistivity: 1.91–1.33 × 10^{-3} Ω cm) were successively washed with water and acetone, and 5% HF aqueous solution to remove possible organic and oxide contaminants. Then a 2.5 nm thick Al film was deposited on the clean GaAs wafer using an electron beam evaporator, followed by the deposition of 300 nm Al_2O_3 as an insulating layer through sputtering with the aid of a shadow mask. To fabricate AlO_x passivated BLG/GaAs Schottky NIRPD, BLG films were then transferred onto the top of the substrate, forming a Schottky junction to the GaAs substrate. After that, an Au electrode serving as an electrical contact to BLG was deposited on the substrate using another shadow mask, and an Ag/Sn alloy electrode serving as an Ohmic contact for n-type GaAs was deposited on the back side of the substrate. For comparison, a BLG/GaAs Schottky device without an AlO_x passivation (WO-PD) layer was also fabricated. The BLG was characterized using a Raman spectrometer (JY, LabRAM HR800). The X-ray photoelectron spectroscopy (XPS, Thermo ESCALAB 250Xi) study was performed using a monochromated Al Kα X-ray source. The electrical properties of the Schottky junction NIRPDs were studied using a semiconductor characterization system (Keithley 4200-SCS). To determine the spectral response and time response of the Schottky devices, a home-built system composed of a monochromator (LE-SP-M300), an oscilloscope (Tektronix, TDS2012B), and a pulsed LED with frequency as high as 1 MHz was used.

Fig. 1(a) shows the schematic illustration of the proof-of-concept BLG/GaAs Schottky NIRPD with an AlO_x passivation layer (W-PD). Owing to the distinct difference in contrast, these three layers can be easily distinguished from the SEM images (Fig. 1(b)). Raman analysis of the BLG film reveals two obvious peaks, *i.e.*, a 2D band peak at ~2670 cm^{-1} and a G band peak at ~1580 cm^{-1} (Fig. 1(c)). The intensity ratio of $I_{2D} : I_G \approx 1.1$ confirms the high crystal quality of the bilayer graphene film.[21] In addition, the weak D peak at ~1350 cm^{-1} signifies a very low amount of defects.[22] Fig. 1(d) shows the XPS spectrum of the GaAs substrate after coating with an AlO_x passivation layer. There are only two sharp Al peaks with a binding energy of 74.4 and 118.8 eV, which can be assigned to the 2p and 2s of three-valence aluminum, respectively, suggesting that the as-deposited Al film in zero-valence has been completely oxidized to Al oxide. Fig. 1(e) shows the XRD patterns with and without passivation, from which no obvious shift or new peaks were observed, suggesting that the crystallinity of GaAs has not been influenced by the introduction of ultra-thin AlO_x. Further photoluminescence analysis reveals that the spectrum intensity of the GaAs with AlO_x passivation is slightly higher than that without surface passivation (Fig. 1(f)). As we will discuss later, such an increase in intensity is due to the reduced recombination of charge carriers at the GaAs surface.

Fig. 2(a) plots a typical current–voltage (*I–V*) curve of both W-PD and WO-PD in the dark. It is obvious that both devices display typical rectifying behavior. The rectification ratios are 134

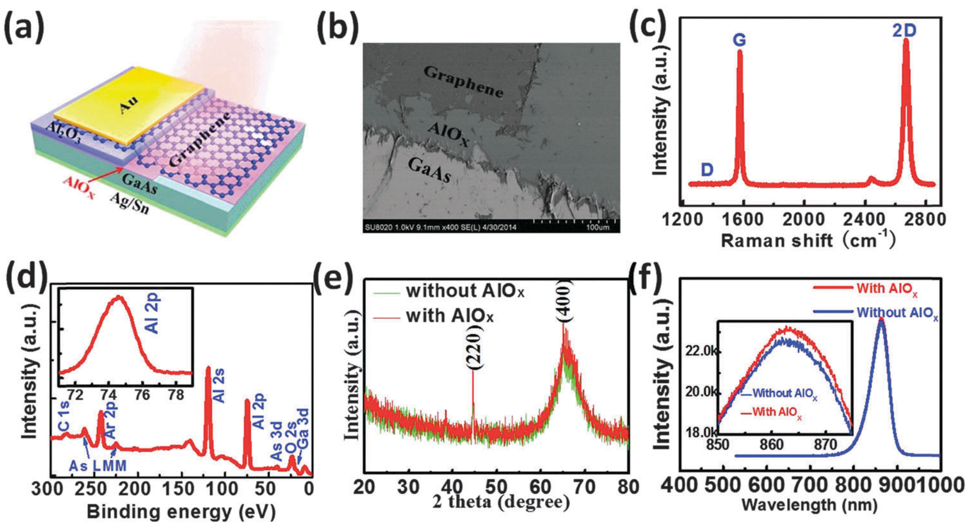

Fig. 1 (a) Schematic illustration of the BLG/GaAs Schottky junction NIRPD with an AlO_x passivation layer. (b) A typical SEM image of the BLG/GaAs Schottky junction with an AlO_x passivation layer. (c) Raman spectrum of the BLG. (d) XPS spectrum of the 2.5 nm Al deposited on the GaAs substrate, the inset shows the corresponding Al 2p spectrum. (e) XRD pattern with and without AlO_x passivation. (f) The photoluminescence of GaAs with and without the AlO_x layer, the inset shows the enlarged spectrum.

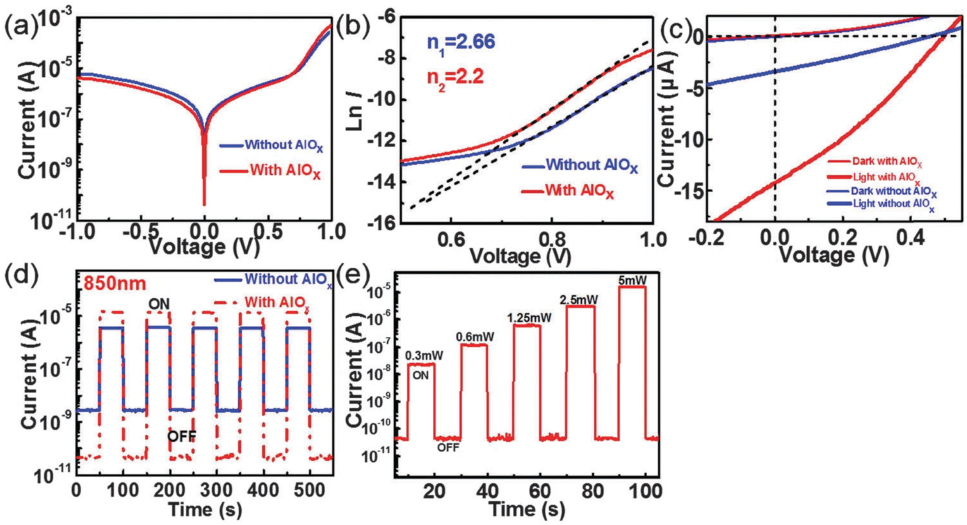

Fig. 2 (a) Typical I–V characteristics of the BLG/GaAs Schottky junction with and without an AlO_x passivation layer under ambient conditions in the dark. (b) Plots of ln I–V showing the ideality factors of both devices. (c) The photovoltaic characteristics of both devices. (d) The photoresponse of both devices illuminated by an 850 nm light source. This study is measured at zero bias voltage, and the incident light intensity is kept at 3 mW cm^{-2}. (e) Photocurrent as a function of incident light intensity.

and 49 at ±1 V for W-PD and WO-PD, respectively. By fitting the ln$I$–V plots shown in Fig. 2(b), the ideality factor of W-PD is determined to be 2.4, comparable to that of WO-PD (2.66). Additionally, the Schottky barriers of both W-PD and WO-PD can be calculated to be 0.68 and 0.59 eV, respectively, by using the thermionic-emission theory: $J(V,T) = J(T)_{\mathrm{S}}\left[\exp\left(\dfrac{eV}{nk_{\mathrm{B}}T}\right)-1\right]$,[23] where $J(T, V)$ is the current density across the device interface, V the applied voltage, k_{B} Boltzmann's constant, T the absolute temperature, and n the ideality factor$\left(n = \dfrac{q}{kT}\dfrac{\mathrm{d}V}{\mathrm{d}\ln I}\right)$. This electrical analysis suggests that the rectification behavior of the BLG/GaAs Schottky junction is well-preserved after surface passivation with an ultrathin AlO_x layer.

To study the effect of surface passivation on device performance, the photoresponse characteristics of the two devices were investigated under the same irradiation. Fig. 2(c) compares the I–V curves of both devices illuminated using an 850 nm light source with a fixed intensity of 3 mW cm^{-2}. Apparently, the device with an AlO_x layer exhibits more pronounced photovoltaic characteristics compared to that without passivation. It is believed that the effective suppression of recombination activities at the GaAs surface, as a result of reduced density of surface dangling bonds and defects after AlO_x passivation is responsible for the improved device photovoltaic performance.[24] In order to quantify the interface defect density in the passivated and un-passivated devices, the interface G_{ss}–f measurement was conducted. Fig. 3 shows the G_{ss}/ω *versus* ω ($\omega = 2\pi f$) curve in a semi-logarithmic scale at a forward bias voltage of +1 V. The interface state density can be deduced from the G_{ss}/ω *versus* ω curve by using the following expression

$$\frac{G_{\mathrm{SS}}}{\omega} = \frac{SqD_{\mathrm{it}}}{2\omega\tau}\ln\left(1+\omega^2{\tau_{\mathrm{it}}}^2\right)$$

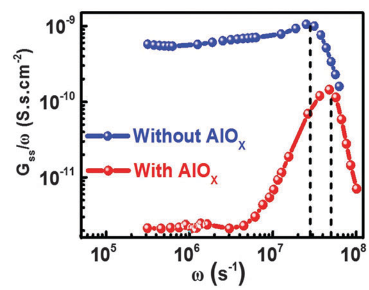

Fig. 3 The G_{ss}/ω *versus* ω ($\omega = 2\pi f$) curve of devices with and without an AlO_x passivation layer in the semi-logarithmic scale at a forward bias voltage of 1 V.

where S is the diode contact area, D_{it} the concentration of trapping states, q the electronic charge, and τ_{it} the time constant of the interface states. At the peak position, ω for the un-passivated and passivated GaAs is 2.73×10^7 and 4.9×10^7 s^{-1}, respectively. When $\dfrac{\mathrm{d}(G_{\mathrm{SS}}/\omega)}{\mathrm{d}(\omega)} = 0$, D_{it} for the un-passivated and passivated GaAs surface is calculated to be 1.5×10^{10} and 2.2×10^9 cm^{-2} eV^{-1}, respectively. These trapping states may originate from the surface defects on the GaAs surface, which can be considerably reduced by the interfacial passivation.

Notably, the AlO_x interfacial passivation layer is highly beneficial for NIR detection. As illustrated in Fig. 2(d), when the light was switched on and off repeatedly at zero bias voltage, both devices can be reversibly switched between low- and high-resistivity states. A careful examination of the photoresponse concluded that the AlO_x passivation can cause a considerable increase in photocurrent (from 3.4×10^{-6} to 1.5×10^{-5} A) and a decrease in dark current (from 2.7×10^{-9} to 4.3×10^{-11} A), giving rise to an on–off ratio as high as

3.0×10^5, which is much higher than 1.2×10^3 of the WO-PD. Such an increase in the on–off ratio is primarily due to the surface passivation of the AlO_x layer, which can substantially reduce the density of dangling bonds and defect states at the GaAs surface, leading to the reduction of the recombination rate that is proportional to the defect density at the GaAs surface. As a result, more carriers are collected by the bottom Ag/Sn alloy electrode and graphene under light illumination.[25,26] On the other hand, the AlO_x interface passivation layer can act as a barrier to prevent electron transport and reduce the leakage current effectively in the dark, leading to decreased dark current.[27] What is more, the photocurrent of the passivated device displays high dependence on the intensity of excitation light. Fig. 2(e) plots the photocurrent under light irradiation with varied intensity, from which one can see that the photocurrent of the device increases gradually with increasing light intensity.

To evaluate the influence of the passivation layer on photoresponse in a more quantitative way, we calculated the other critical parameters, the responsivity (R) and detectivity (D^*) which can be described as $R(\mathrm{AW^{-1}}) = \dfrac{I_\mathrm{p} - I_\mathrm{d}}{P_\mathrm{opt}}$ and $D^* = \sqrt{\dfrac{A}{2qI_\mathrm{d}}}R$, respectively. In the equations, I_p, I_d, P_opt, A, and q are the photocurrent, dark current, incident light power, active area, and elementary charge, respectively. The device area was estimated to be $\sim$0.03 cm^2. Based on these values, the responsivity (R) and detectivity (D^*) of the WO-PD are estimated to be 1.2 mA W^{-1} and 7.3×10^9 cm Hz$^{1/2}$ W^{-1}, respectively. Upon deposition of the AlO_x passivation layer, R and D^* increased to 5 mA W^{-1} and 2.88×10^{11} cm Hz$^{1/2}$ W^{-1}, respectively. In addition to the high responsivity and detectivity, the passivation layer is beneficial to the response rate as well. The schematic illustration in Fig. 4(a) depicts the experimental setup to study the response rate. The pulsed incident light was provided by an LED (850 nm) driven by a high-frequency power supply. The fast-varying signal from the NIRPDs was collected using an oscilloscope. Fig. 4(b) shows the reversible switching of W-PD under the light with a frequency of 1 kHz and 1 MHz. The response is very fast, with good reproducibility and excellent stability. Further study showed that the W-PD has a slow relative balance $[I_\mathrm{max} - I_\mathrm{min}/I_\mathrm{max}]$ decay. As illustrated in Fig. 4(c), the relative balance of W-PD remained larger than 60% even when the frequency was increased to 10 kHz, in stark contrast to that of WO-PD. By fitting a single normalized cycle shown in Fig. 4(d), the rise time (τ_r) and a fall time (τ_f) for W-PD are estimated to be 320 and 380 ns, respectively, which are far faster than those of WO-PD (τ_r: 32 μs and τ_f of 48 μs). Table 1 summarizes the key parameters of our devices with other IRPDs. One can see clearly that although the current device is relatively weak in responsivity, other key parameters including the on/off ratio and detectivity are much higher than those of similar devices such as core–shell GaAs/AlGaAs/Pt Schottky junctions,[11] graphene/Ge wafers,[14] GaAs nanocone array/MLG array Schottky junctions,[17] and Si/MLG heterojunctions.[28]

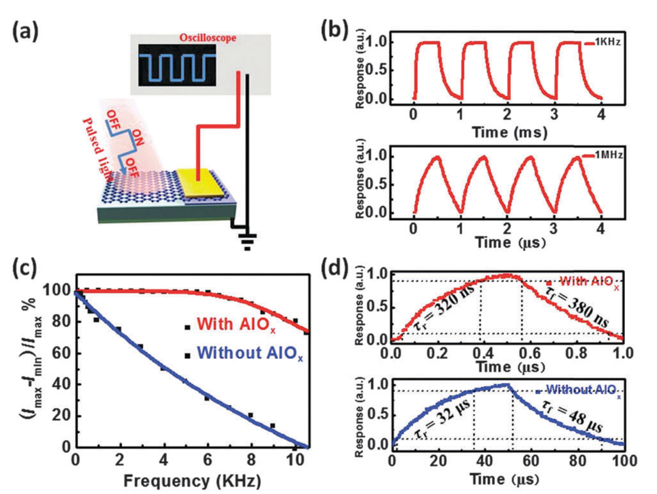

Fig. 4 (a) Schematic illustration of our experimental setup for the NIRPD response rate measurement. (b) Response of the BLG/GaAs Schottky junction with the AlO_x layer to pulsed NIR light at frequencies of 1 kHz and 1 MHz. (c) The relative balance *versus* switching frequency of the pulsed NIR light. (d) A single normalized cycle to estimate both rise time (τ_r) and fall time (τ_f) of the NIRPD with and without AlO_x.

The ultrafast response rate can be attributed to the suppression of carrier trapping after AlO_x passivation, which can substantially reduce the density of the surface states (*e.g.*, surface's dangling bonds and surface defects).[29] Fig. 5 shows the energy band diagram of the BLG/GaAs Schottky junction with an ultrathin AlO_x passivation layer under light illumination at zero bias voltage. When irradiated by NIR, the photogenerated electron–hole pairs are quickly separated by the built-in electric field. The photo-induced electrons can be collected using an Ag/Sn electrode, while the holes in contrast are collected by BLG through tunneling, leading to the formation of photocurrent. During this process, the ultrathin AlO_x layer can reduce the density of recombination centers by terminating the surface states of GaAs. Thus the recombination activity is considerably reduced, giving rise to enhanced photocurrent and responsivity.

Table 1 Comparison of the device performance of the present device with other NIRPDs

Device structure	Responsivity (mA W^{-1})	$\tau_\mathrm{r}/\tau_\mathrm{f}$	$I_\mathrm{light}/I_\mathrm{dark}$	Detectivity (Jones)	Ref.
BLG/GaAs Schottky junction with AlO_x interface passivation layer	5	380/320 ns	10^5	2.88×10^{11}	This work
BLG/GaAs Schottky junction	1.2	32/48 μs	10^5	7.3×10^9	This work
Graphene/Ge wafer	50	23/108 μs	10^5	1.38×10^{10}	13
Core–shell GaAs/AlGaAs/Pt Schottky junction	570	—	—	7.2×10^{10}	11
GaAs nanocone array/MLG array Schottky junction	1.73	72/122 μs	10^4	1.83×10^{11}	16
Si/MLG heterojunction	435	1.2/3 ms	10^4	7.69×10^9	31

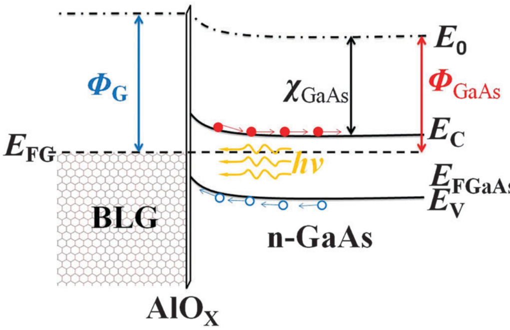

Fig. 5 Energy band diagram of the NIRPD under light illumination.

According to the above analysis, the passivation layer plays an important role in determining the performance of the NIR detector. The thickness of the passivation layer is the key to device optimization. Fig. 6(a) plots the *I–V* curves of a number of devices coated by AlO_x with thickness in the range from 0 to 8.5 nm. Obviously, the device with a 2.5 nm thick passivation layer shows the highest photocurrent. A further increase in thickness will lead to reduced photocurrent. This decrease in photocurrent can be ascribed to the blocking effect of thick AlO_x, which will prevent the separation of carrier transfer under light illumination. In this study, we have also studied the passivation effect of SiO_2 and Si_3N_4 layers, which were evaporated using an electron beam evaporator. As plotted in Fig. 6(b), their performance is not as good as that passivated with the AlO_x layer. The detailed reason for this phenomenon is still unknown to us. Finally, it should be noted that the present NIR photodetector shows excellent stability even after long-term storage under ambient conditions. Fig. 6(c) compares the *I–V* characteristics after nearly one month storage. There is no obvious degradation in device performance, suggesting that this device has a long lifetime.

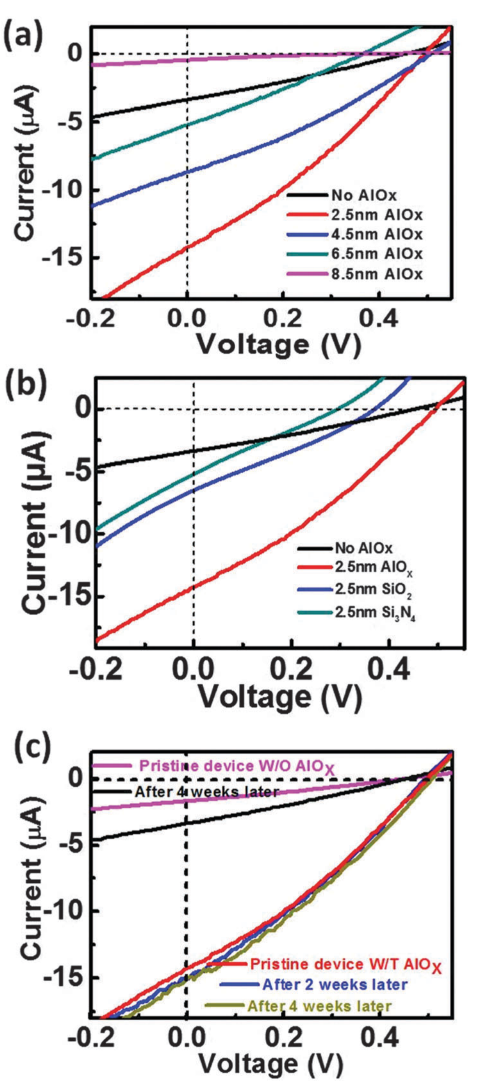

Fig. 6 The photovoltaic characteristics of the BLG/GaAs Schottky junction coated by: (a) an AlO_x passivation layer with different thickness; (b) different passivation layer; and (c) an AlO_x passivation layer after long-term storage.

In conclusion, we have demonstrated a high-performance NIRPD based on the BLG/GaAs Schottky junction using an AlO_x passivation layer. Optoelectronic analysis reveals that the AlO_x passivated NIRPD exhibits high sensitivity to 850 nm illumination at zero bias voltage. The dark current was reduced considerably, while the responsivity was increased after passivation. It is also observed that the detectivity of the NIRPD with AlO_x was estimated to be 2.88×10^{11} cm $Hz^{1/2}$ W^{-1}, respectively, which is much higher than that without AlO_x passivation. In addition, further device analysis shows that the passivated NIRPD can work in an ultra-wide range of switching frequencies, with an ultra-fast response rate (τ_r = 320 ns, τ_f = 380 ns), which is far faster than those of WO-PD. It is expected that this simple BLG/GaAs Schottky junction with an AlO_x passivation layer will have potential applications in the future NIR detection.

Acknowledgements

This work was supported by the Natural Science Foundation of China (NSFC, No. 51172151, 21101051), the Fundamental Research Funds for the Central Universities (2012HGCX0003, 2013HGCH0012, 2014HGCH0005), the China Postdoctoral Science Foundation (103471013), and the Natural Science Foundation of the Anhui Province (Grant No. J2014KZR0059 and J2014KZR0042).

References

1 A. Rogalski, *Infrared Detectors*, CRC Press, Florida, USA, 2nd edn, 2010.
2 G. Yu, Z. Liu, X. M. Xie, X. Ouyang and G. Shen, Flexible Photodetector with Single-Crystalline GaTe Nanowires, *J. Mater. Chem. C*, 2014, **2**, 6104–6110.
3 M. Casalino, L. Sirleto, M. Iodice, N. Saffioti, M. Gioffrè, I. Rendina and G. Coppola, Cu/p-Si Schottky Barrier-Based Near Infrared Photodetector Integrated with a Silicon-on-Insulator Waveguide, *Appl. Phys. Lett.*, 2010, **96**, 241112.
4 M. R. Hao, Y. Yang, S. Zhang, W. Z. Shen, H. Schneider and H. C. Liu, Near-Room-Temperature Photon-Noise-Limited

Quantum Well Infrared Photodetector, *Laser Photonics Rev.*, 2014, **8**, 297–302.

5 C. J. Chen, K. K. Choi, W. H. Chang and D. C. Tsui, Corrugated Quantum Well Infrared Photodetectors with Polyimide Planarization for Detector Array Applications, *IEEE Trans. Electron Devices*, 1998, **45**, 1431–1437.

6 S. Keuleyan, E. Lhuillier, V. Brajuskovic and P. G. Sionnest, Mid-Infrared HgTe Colloidal Quantum Dot Photodetectors, *Nat. Photonics*, 2011, **5**, 489–493.

7 J. Wang, X. S. Chen, W. D. Hu, L. Wang, W. Lu, F. Q. Xu, J. Zhao, Y. L. Shi and R. B. Ji, Amorphous, HgCdTe Infrared Photoconductive Detector with High Detectivity above 200 K, *Appl. Phys. Lett.*, 2011, **99**, 113508.

8 P. S. Wijewarnasuriya, Y. Chen, G. Brill, B. Zandi and N. K. Dhar, High-Performance Long-Wavelength Infrared HgCdTe Focal Plane Arrays Fabricated on CdSeTe Compliant Si Substrates, *IEEE Trans. Electron Devices*, 2010, **57**, 782–787.

9 J. Yoon, S. Jo, I. S. Chun, I. Jung, H. S. Kim, M. Meitl, E. Menard, X. L. Li, J. J. Coleman, U. Paik and J. A. Rogers, GaAs Photovoltaics and Optoelectronics Using Releasable Multilayer Epitaxial Assemblies, *Nature*, 2010, **465**, 329–333.

10 D. Ban, H. Luo, H. C. Lui, Z. R. Wasilewski, Y. Paltiel, A. Raizman and A. Sher, Midinfrared Optical Upconverter, *Appl. Phys. Lett.*, 2005, **86**, 201103.

11 X. Dai, S. Zhang, Z. L. Wang, G. Adamo, H. Liu, Y. Z. Huang, C. Couteau and C. Soci, GaAs/AlGaAs Nanowire Photodetector, *Nano Lett.*, 2014, **14**, 2688–2693.

12 C. Y. Yan, N. Singh, H. Cai, C. L. Gan and P. S. Lee, Network-Enhanced Photoresponse Time of Ge Nanowire Photodetectors, *ACS Appl. Mater. Interfaces*, 2010, **2**, 1794–1797.

13 M. W. Knight, H. Sobhani, P. Nordlander and N. J. Halas, Photodetection with Active Optical Antennas, *Science*, 2011, **332**, 702–704.

14 L. H. Zeng, M. Z. Wang, H. Hu, B. Nie, Y. Q. Yu, C. Y. Wu, L. Wang, J. G. Hu, C. Xie, F. X. Liang and L. B. Luo, Monolayer Graphene/Germanium Schottky Junction as High-Performance Self-Driven infrared Light Photodetector, *ACS Appl. Mater. Interfaces*, 2013, **5**, 9362–9366.

15 L. B. Luo, L. H. Zeng, C. Xie, Y. Q. Yu, F. X. Liang, C. Y. Wu, L. Wang and J. G. Hu, Light Trapping and Surface Plasmon Enhanced High-Performance NIR Photodetector, *Sci. Rep.*, 2014, **4**, 3914.

16 H. Wang, High Gain Single GaAs Nanowire Photodetector, *Appl. Phys. Lett.*, 2013, **103**, 093101.

17 L. B. Luo, J. J. Chen, M. Z. Wang, H. Hu, C. Y. Wu, Q. Li, L. Wang, J. A. Huang and F. X. Liang, Near-Infrared Light Photovoltaic Detector based on GaAs Nanocone Array/Monolayer Graphene Schottky Junction, *Adv. Funct. Mater.*, 2014, **24**, 2794–2800.

18 T. Manago, S. Miyanishi, H. Akinaga, W. V. Roy, R. F. B. Roelfsema, T. Sato and E. Tamura, Schottky Barrier Height of MnSb(0001)/GaAs(111)B Contacts: Influence of Interface Structure, *J. Appl. Phys.*, 2000, **88**, 2043.

19 H. Y. Liu, W. C. Hsu, B. Y. Chou and Y. H. Wang, A Simple Passivation Technique for AlGaN/GaN Ultraviolet Schottky Barrier Photodetector, *IEEE Photonics Technol. Lett.*, 2014, **26**, 138–141.

20 Q. Chen, H. Y. Ding, Y. K. Wu, M. Q. Sui, W. Lu, B. Wang, W. M. Su, Z. Cui and L. W. Chen, Passivation of Surface States in the ZnO Nanowire with Thermally Evaporated Copper Phthalocyanine for Hybrid Photodetectors, *Nanoscale*, 2013, **5**, 4162–4165.

21 X. S. Li, W. W. Cai, J. H. An, S. Y. Kim, J. H. Nah, D. X. Yang, R. Piner, A. Velamakanni, I. H. Jung, E. Tutuc, S. K. Banerjee, L. Colombo and R. S. Ruoff, Large-Area Synthesis of High-Quality and Uniform Graphene Films on Copper Foils, *Science*, 2009, **324**, 1312–1314.

22 A. C. Ferrari, J. C. Meyer, V. Scardaci, C. Casiraghi, M. Lazzeri, F. Mauri, S. Piscanec, D. Jiang, K. S. Novoselov, S. Roth and A. K. Geim, Raman Spectrum of Graphene and Graphene Layers, *Phys. Rev. Lett.*, 2006, **97**, 187401.

23 B. Nie, J. G. Hu, L. B. Luo, C. Xie, L. H. Zeng, P. Lv, F. Z. Li, J. S. Jie, M. Feng, C. Y. Wu, Y. Q. Yu and S. H. Yu, Monolayer Graphene Film on ZnO Nanorod Array for High-Performance Schottky Junction Ultraviolet Photodetector, *Small*, 2013, **9**, 2872–2879.

24 N. Tajik, Z. Peng, P. Kuyanov and R. R. LaPierre, Sulfur Passivation and Contact Methods for GaAs Nanowire Solar Cells, *Nanotechnology*, 2011, **22**, 225402.

25 B. Hoex, J. Schmidt, P. Pohl, M. C. M. van de Sanden and W. M. M. Kessels, Silicon Surface Passivation by Atomic Layer Deposited Al_2O_3, *J. Appl. Phys.*, 2008, **104**, 044903.

26 A. G. Aberle, Surface Passivation of Crystalline Silicon Solar Cells: A Review, *Prog. Photovoltaics*, 2000, **8**, 473–487.

27 V. Adivarahan, G. Simin, J. W. Yang, A. Lunev and M. Asif Khan, SiO_2-Passivated Lateral-Geometry GaN Transparent Schottky-Barrier Detectors, *Appl. Phys. Lett.*, 2000, **77**, 863.

28 X. H. An, F. Z. Liu, Y. J. Jung and S. Kar, Tunable Graphene-Silicon Heterojunctions For Ultrasensitive Photodetection, *Nano Lett.*, 2013, **13**, 909–916.

29 C. Xie, B. Nie, L. H. Zeng, F. X. Liang, M. Z. Wang, L. B. Luo, M. Feng, Y. Q. Yu, C. Y. Wu, Y. C. Wu and S. H. Yu, Core–Shell Heterojunction of Silicon Nanowire Arrays and Carbon Quantum Dots for Photovoltaic Devices and Self-Driven Photodetectors, *ACS Nano*, 2014, **8**, 4015–4022.

